Journal of Materials Chemistry A

PAPER

View Article Online
View Journal | View Issue

Cite this: J. Mater. Chem. A, 2016, 4, 17073

Robust bioinspired graphene-based nanocomposites *via* synergistic toughening of zinc ions and covalent bonding†

Shanshan Gong, Lei Jiang and Qunfeng Cheng*

Received 12th August 2016
Accepted 6th October 2016

DOI: 10.1039/c6ta06893f

www.rsc.org/MaterialsA

Published on 07 October 2016. Downloaded on 06/11/2016 06:08:16.

Robust graphene-based nanocomposites show promising applications in fields of flexible, wearable and intelligent devices. But, it is still a big challenge to construct high performance macroscopic graphene-based nanocomposites for practical application through cost-efficient graphene oxide (GO) nanosheets. Inspired by the hierarchical layered structure and interfacial interactions of nacre, we demonstrated robust graphene-based nanocomposites *via* synergistic interfacial interactions, which are constructed *via* divalent ions of zinc (Zn^{2+}), and linear molecules of 10,12-pentacosadiyn-1-ol (PCDO) with GO nanosheets. The synergistic interfacial interactions result in integrated high strength, toughness and fatigue life. Furthermore, the resultant bioinspired graphene-based nanocomposites (BGBNs) also possess high electrical conductivity. The extraordinary performance allows this kind of BGBN to be potentially utilized in aerospace, flexible electrodes of supercapacitors and other intelligent devices. The demonstration of synergistic interfacial interactions of ionic and covalent bonding also supplies an effective approach for building robust graphene-based nanocomposites in the future.

Biological materials, such as bone, spider silk and nacre, feature exceptional mechanical performance, including high tensile strength, super toughness and admirable extensibility.[1,2] These extraordinary performances are attributed to their sophisticated architectures with hierarchical nano- and molecular-scales.[3,4] Natural nacre possesses a high interfacial performance due to its surface roughness and a few percent of resilient organic materials,[4] as well as extrinsic toughening mechanisms, such as crack deflection and crack bridging.[5] Therefore, to obtain high toughness, the designing and assembling of nacre-like materials are tremendously accelerated.[5] Graphene oxide (GO), a derivative of graphene, is a fascinating building block for fabricating laminated nacre-like materials.[6–10] Recently, many bioinspired graphene-based nanocomposites (BGBNs) with different interfaces have been assembled widely. Usually, there exist four types of interfacial interactions for assembling BGBNs,[11,12] such as hydrogen bonding, ionic bonding, π–π interaction, and covalent bonding, respectively. For example, hydrogen bonding networks were built in BGBNs with poly(vinyl alcohol) (PVA)[13] and hydrophobic poly(methyl methacrylate) (PMMA)[14] (reduced graphene oxide (rGO)–PVA,[13] GO–PMMA[14]). Some metal ions, containing Ca^{2+},[15] Al^{3+},[16] and Cu^{2+},[17] have also been demonstrated to cross-link GO nanosheets for achieving BGBNs (GO–Ca^{2+},[15] GO–Al^{3+},[16] and GO–Cu^{2+} (ref. 17)). The π–π interactions are also introduced to fabricate BGBNs through pyrene and its derivatives cross-linking reduced GO nanosheets.[18]

However, it is difficult to simultaneously achieve ultrahigh strength and toughness of BGBNs *via* a single interfacial interaction. The synergistic effect of interfacial interactions exists in natural materials, demonstrating it as an essential factor to improve BGBNs' strength and toughness simultaneously,[11,19,20] for example, rGO–chitosan (CS) with synergy of hydrogen and covalent bonding.[21] In fact, trace amounts of metal ions could result in extraordinary mechanical properties when introduced into the protein structures of natural materials.[22] For example, zinc (Zn^{2+}) ions have been revealed to improve the mechanical properties of the jaws in Nereis.[23,24] In addition, Zn^{2+} ions have been demonstrated to dramatically improve the mechanical properties of spider silk.[22]

Herein, we demonstrated that the synergistic interfacial interactions of ionic and covalent bonding are utilized to improve the mechanical properties of BGBNs. The ionic bonding is introduced *via* Zn^{2+} with GO nanosheets, which forms a synergistic toughening effect with covalent bonding by 10,12-pentacosadiyn-1-ol (PCDO) long linear chain molecules. The resultant BGBNs show a high tensile strength of 439.1 ± 15.9 MPa and toughness of 7.6 ± 0.5 MJ m^{-3}, higher than those of natural nacre,[3] respectively. Moreover, the robust BGBNs also possess long fatigue life and outstanding electrical conductivity. These extraordinary properties may enable these new BGBNs for

Key Laboratory of Bio-inspired Smart Interfacial Science and Technology of Ministry of Education, School of Chemistry and Environment, Beihang University, Beijing 100191, P. R. China. E-mail: cheng@buaa.edu.cn

† Electronic supplementary information (ESI) available. See DOI: 10.1039/c6ta06893f

Published on 07 October 2016. Downloaded on 06/11/2016 06:08:16.

a variety of applications in aerospace, flexible electrodes of supercapacitors and other intelligent devices. This synergistic toughening approach with ionic and covalent bonding also provides an alternative approach for fabricating high performance multifunctional BGBNs in the near future.

Results and discussion

The thickness of exfoliated GO nanosheets is about 1.0 nm, as shown in Fig. S1.† The fabrication process of the BGBNs with cross-linking of Zn^{2+} and PCDO is illustrated in Fig. 1a. First, the GO nanosheets/Zn^{2+} homogeneous suspension was assembled into layered films (GO–Zn^{2+}) by vacuum-assisted filtration. Two types of coordinations occurred between Zn^{2+} and the oxygenated functional groups of the GO nanosheets:[25] (i) bridging at the edges of GO nanosheets, and (ii) intercalation between the adjacent GO nanosheets. Then, the obtained GO–Zn^{2+} films were immersed into the PCDO/tetrahydrofuran (THF) solution. Similar to the previous report,[26] the esterification between GO nanosheets and PCDO molecules happened during this process. Furthermore, after ultraviolet irradiation,[27] 1,4-addition polymerization occurred between the PCDO long linear molecules. Then the GO–Zn^{2+}–PCDO nanocomposites with Zn^{2+} ionic bonding and PCDO covalent cross-linking were obtained. Finally, the resultant BGBNs of rGO–Zn^{2+}–PCDO were achieved after chemical reduction using hydroiodic acid (HI),[28] and the digital photograph is shown in Fig. 1b. The cross-sectional and surface fracture morphologies of the rGO–Zn^{2+}–PCDO nanocomposites exhibit orderly layered nacre-like structures, as shown in Fig. 1c and d.

To optimize the content effect of Zn^{2+} on the mechanical properties of GO–Zn^{2+} layered materials, several weight ratios of Zn^{2+} were selected, including 0.50 wt% (GO–Zn^{2+}-I), 1.00 wt% (GO–Zn^{2+}-II), 3.00 wt% (GO–Zn^{2+}-III) and 5.00 wt% (GO–Zn^{2+}-IV), respectively. The confirmed contents of Zn^{2+} by thermogravimetric analysis (TGA) were about 0.44 wt%, 0.95 wt%, 2.33 wt% and 4.30 wt%, respectively, which are listed in Table S1.† Fig. S2a† shows the corresponding TGA curves. Moreover, the content of PCDO in GO–Zn^{2+}–PCDO-I nanocomposites was confirmed by TGA about 2.68 wt%, as shown in Fig. S2b.† X-ray diffraction (XRD) is conducted to verify the successful introduction of both Zn^{2+} and PCDO molecules, as shown in Fig. S3.† For example, the *d*-spacing of GO–Zn^{2+}-IV nanocomposites increased to 8.32 Å from 7.52 Å for the pure GO film (Fig. S3a†), as well as the *d*-spacing of GO–Zn^{2+}–PCDO-IV nanocomposites increased to 8.61 Å from 7.61 Å for GO–Zn^{2+}–PCDO-I nanocomposites (Fig. S3b), which are also listed in Table S2.† Fig. 2a shows the results of Fourier transform infrared (FTIR) spectra. Before coordination with Zn^{2+}, there exist five characteristic peaks within the range of 1900–900 cm^{-1}, for example, carboxyl/carbonyl C=O (1690–1740 cm^{-1}), aromatic ring C=C (1430–1650 cm^{-1}), carboxyl C–O (~1400 cm^{-1}), epoxide/ether C–O (~1230 cm^{-1}), and alkoxy C–O (~1050 cm^{-1}). After Zn^{2+} coordination, the stretching vibration of C=O at

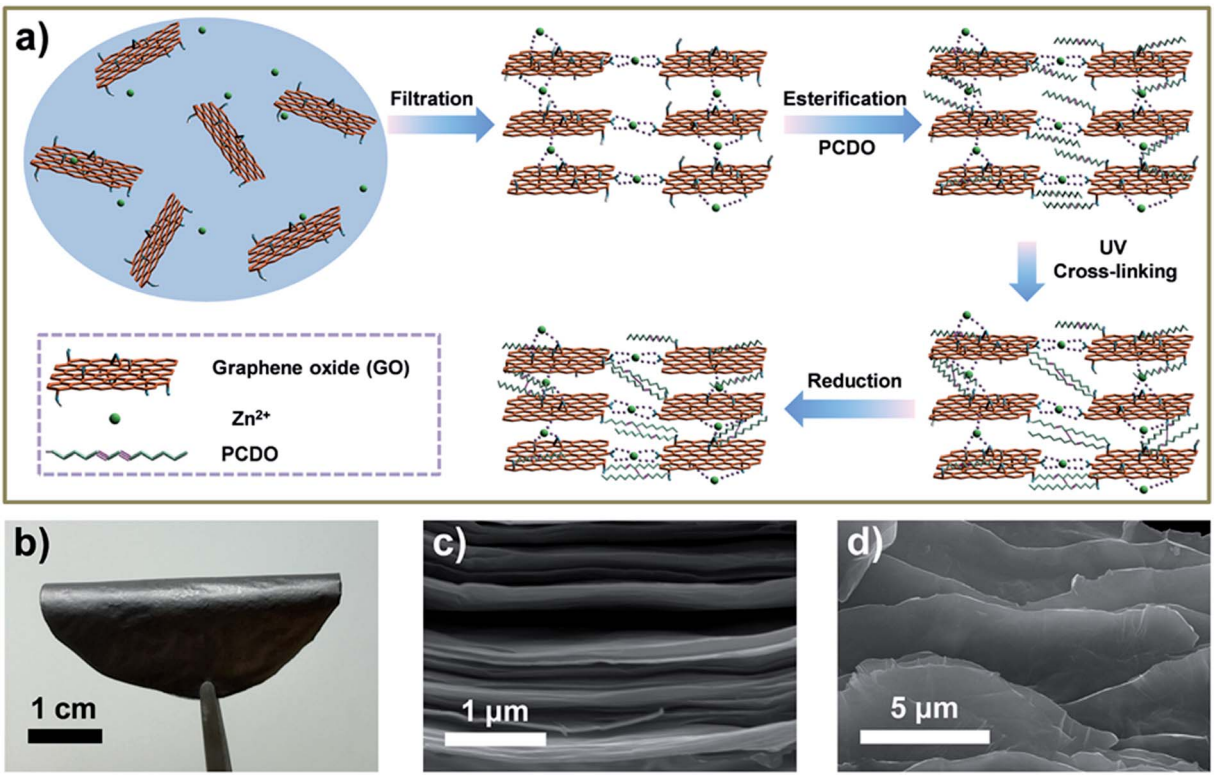

Fig. 1 (a) and (b) Fabrication process and digital photograph of the rGO–Zn^{2+}–PCDO nanocomposites. (c) and (d) Cross-section and fracture surface morphologies of the rGO–Zn^{2+}–PCDO nanocomposites, indicating orderly layered nacre-like structures and edge curling of rGO nanosheets after tensile testing.

 This journal is © The Royal Society of Chemistry 2016

Published on 07 October 2016. Downloaded on 06/11/2016 06:08:16.

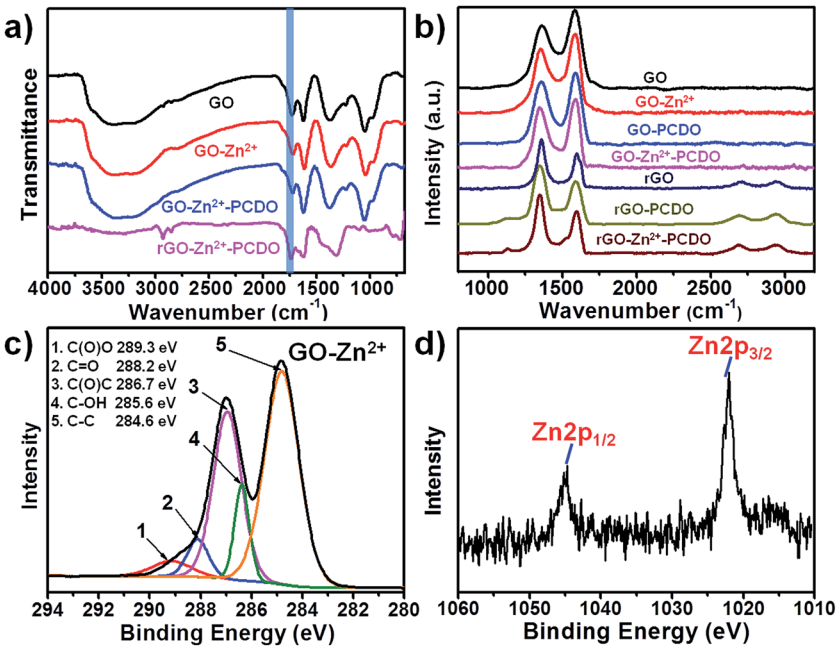

Fig. 2 (a) FTIR spectra of pure GO, GO–Zn^{2+}-I, GO–Zn^{2+}–PCDO-I and rGO–Zn^{2+}–PCDO-I nanocomposites. (b) Raman spectra comparison. (c) XPS spectra of the GO–Zn^{2+}-I nanocomposites with C–C, C–OH, C(O)C, C=O and C(O)O groups. (d) The binding energy of Zn $2p_{1/2}$ and Zn $2p_{3/2}$ at 1044.8 eV and 1022.1 eV, respectively. The above results demonstrate that both divalent zinc ions and PCDO successfully cross-linked with the GO nanosheets in the resultant nanocomposites.

1728 cm^{-1} decreased, which is direct evidence that the coordination occurred between carboxylic acid and Zn^{2+}.[15,29] In addition, the relative intensity of the peak at 1227 cm^{-1} for epoxide C–O decreased, as well as obvious increasing peak intensity for alkoxy C–O at 1045 cm^{-1}, suggesting the ring-opening coordination.[15,30] After grafting of the PCDO molecules, the characteristic peak of C=O at 1728 cm^{-1} weakened again and shifted to 1720 cm^{-1},[26] which demonstrates esterification between PCDO molecules and GO nanosheets. Raman spectra show the gradual increase of I_D/I_G, indicating cross-linking with Zn^{2+} bonding and PCDO molecules chemically cross-linking with adjacent GO nanosheets, shown in Fig. 2b.

Fig. 2c and S4† show X-ray photoelectron spectroscopy (XPS) results. Compared with the pure GO film, the C_{1s} component of C(O)O in the GO–Zn^{2+}-I nanocomposites slightly shifts to 289.1 eV from 289.3 eV, indicating the complexation between carboxylic acid groups and divalent zinc ions.[31] In addition, the C(O)C group at 286.7 eV slightly decreases and C–OH at 285.6 eV shows a significant increase, further confirming that the epoxides undergo ring-opening and C–OH groups are generated.[15] The XPS spectrum of the GO–Zn^{2+}-I nanocomposites also exhibits two peaks at 1044.8 eV and 1022.1 eV, corresponding to the binding energies of Zn $2p_{1/2}$ and Zn $2p_{3/2}$ (Fig. 2d). The peak intensity of the oxygenated functional groups in the rGO–Zn^{2+}–PCDO-I nanocomposites decreases dramatically after chemical reduction, as shown in Fig. S4c.†

The stress–strain curves of the pure GO film (curve 1), rGO film (curve 2), rGO–PCDO (curve 3), rGO–Zn^{2+}-I (curve 4), GO–Zn^{2+}–PCDO-I (curve 5) and rGO–Zn^{2+}–PCDO-I (curve 6) nanocomposites are shown in Fig. 3a. The pure GO film (curve 1) shows a tensile strength of 133.8 ± 7.6 MPa and toughness of 0.8 ± 0.1 MJ m^{-3}, lower than those of nacre,[3] respectively, showing brittle fracture, due to weak interfacial interactions. After chemical reduction, the rGO film (curve 2) shows a high strength of 213.1 ± 9.8 MPa and toughness of 2.2 ± 0.07 MJ m^{-3} with dense laminated structures. And after coordination ionic bonding with Zn^{2+}, the mechanical properties of the binary GO–Zn^{2+} nanocomposites are greatly improved. In fact, the Zn^{2+} content plays a key role in the overall mechanical properties of binary GO–Zn^{2+} nanocomposites. As shown in Fig. S5a and b,† the tensile strength and toughness of GO–Zn^{2+}-I nanocomposites reach maximum values when the Zn^{2+} is about 0.44 wt%, which is consistent with natural materials.[3] Covalent bonding is introduced into binary GO–Zn^{2+} nanocomposites by PCDO molecules, resulting in improvement of interfacial strength. For example, GO–Zn^{2+}–PCDO-I nanocomposites (curve 5) show a tensile strength of 319.7 ± 17.6 MPa and toughness of 5.2 ± 0.4 MJ m^{-3}, higher than those of GO–Zn^{2+}-I nanocomposites with a tensile strength of 287.1 ± 7.9 MPa and toughness of 3.3 ± 0.5 MJ m^{-3}, respectively, as shown in Fig. S5a and b.† Some functional groups are removed from GO nanosheets after chemical reduction; thus the interlayer distance of the rGO–Zn^{2+}–PCDO-I nanocomposites (curve 6) decreases, resulting in a dense layered structure, and a high tensile strength of 439.1 ± 15.9 MPa and toughness of 7.5 ± 0.5 MJ m^{-3} (Fig. 3b and c), which are higher than those of rGO–Zn^{2+}-I nanocomposites (Curve 4, tensile strength of 355.6 ± 20.9 MPa and toughness of 4.2 ± 0.9 MJ m^{-3}) with ionic bonding and rGO–PCDO nanocomposites (Curve 3, tensile strength of 369.9 ± 10.3 MPa and toughness of 4.3 ± 0.5 MJ m^{-3}) with covalent bonding. Therefore, the extraordinary and integrated mechanical properties of the BGBNs are attributed to the

Published on 07 October 2016. Downloaded on 06/11/2016 06:08:16.

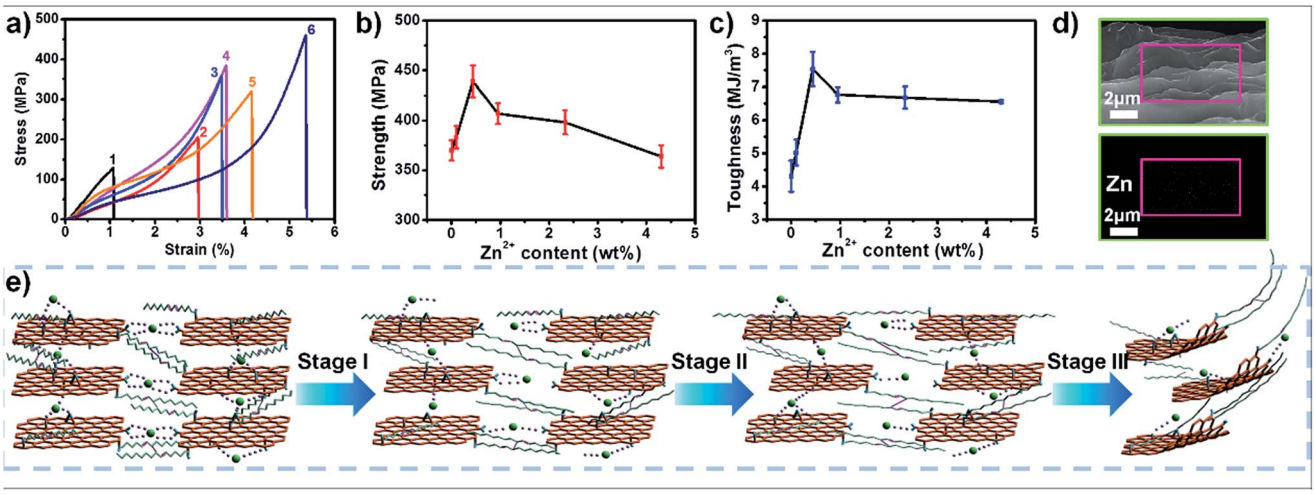

Fig. 3 (a) Typical strain–stress curves of the pure GO film (curve 1), rGO film (curve 2), rGO–PCDO (curve 3), rGO–Zn^{2+}-I (curve 4), GO–Zn^{2+}–PCDO (curve 5) and rGO–Zn^{2+}–PCDO (curve 6) nanocomposites. The tensile strength (b) and toughness (c) of the bioinspired rGO–Zn^{2+}–PCDO nanocomposites with different Zn^{2+} contents. (d) The fracture morphology of the bioinspired rGO–Zn^{2+}–PCDO-I nanocomposites, and the EDS exhibits the uniform distribution of the element Zn in the gallery of the rGO nanosheets. (e) The proposed fracture mechanism of the rGO–Zn^{2+}–PCDO nanocomposites. Stage I: the weak ionic bonds ruptured, accompanying the coiled PCDO molecule chains extending along the sliding direction. Stage II: the PCDO long chains were gradually stretched and weak ionic bonds re-formed. Stage III: the covalent bonds and the re-formed ionic bonds were broken, dissipating much more energy and resulting in the edge curling of the rGO nanosheets.

synergistic effect of Zn^{2+} ionic bonding and covalent bonding. Energy dispersive spectroscopy (EDS) exhibits the distribution of the element Zn in rGO nanosheets of the resultant BGBNs in Fig. 3d, illustrating that the divalent Zn^{2+} ions are uniformly dispersed in the interlayers of rGO nanosheets. The fracture morphologies and details of mechanical properties are listed in Fig. S6 and Table S3.†

In the laminated structure of BGBNs, chelate bonding is formed between rGO nanosheets and Zn^{2+} ions. Simultaneously, the PCDO molecules grafted on rGO nanosheets cross-link with each other into a network through conjugation of ene-yne frameworks.[32] A typical fracture mechanism is proposed to illustrate the synergistic toughening effect of the interfacial interactions in the BGBNs, as shown in Fig. 3e. According to the previous reports,[33,34] the binding energy of covalent bonding is higher than that of ionic bonding;[33] therefore, the strong covalent cross-linking bonding forms a primary network and the weak ionic bonding forms a sacrificial network under loading.[34] When loading (Stage I) the resultant BGBNs, the weak ionic bonds first ruptured,[34] accompanying the coiled PCDO chains extending along the sliding direction and bridging the rGO nanosheets *via* the network of covalent cross-linking. Further loading (Stage II), the PCDO long chains are gradually stretched, while parts of fractured ionic bonds could re-form,[33,35,36] due to the interlayer sliding of the rGO nanosheets. When loading is further increased (Stage III), the covalent bonds are broken and much more energy is dissipated, as well as the breakage of ionic bonds, resulting in curling of the rGO nanosheets. The synergistic toughening of double networks (ionic bonds and covalent bonds) significantly improves mechanical properties of the BGBNs, which is consistent with previous reports.[32,36]

The synergistic toughening of the interfacial interactions also plays a key role in improving fatigue life of BGBNs. The maximum tensile stress (S) *vs.* the number of cycles to failure (N) curves are plotted in Fig. 4a. Compared with the pure rGO film, rGO–PCDO, and rGO–Zn^{2+}-I nanocomposites, the rGO–Zn^{2+}–PCDO-I nanocomposites demonstrated much longer fatigue life at the same stress level. In the process of fatigue testing, rGO nanosheets of rGO–Zn^{2+}–PCDO-I nanocomposites first show crack deflection, and then the covalently cross-linked networks suppress crack propagation by crack bridging, the ionic bonds break as well. Due to the continuous slippage of rGO nanosheets, a part of cracked ionic bonds re-form during a time interval after loading,[33] and the hysteresis phenomenon could further increase energy dissipation.[35] Finally, all of the networks break after tens of thousands of cycles. The synergistic effect of crack bridging with covalent cross-linking and hysteresis from unzipping of ionic bonding, as well as crack deflection of rGO nanosheets, tremendously improves the fatigue-resistance performance of the BGBNs.[36] The corresponding stress–strain fatigue curves are shown in Fig. S7.†

Compared with natural nacre[3] and other layered graphene-based materials, this kind of resultant BGBN shows integrated high strength and toughness due to synergistic interfacial interactions, which is shown in Fig. 4b and Table S4.† The maximum tensile strength and toughness of the rGO–Zn^{2+}–PCDO-I nanocomposites reach 460.5 MPa and 8.1 MJ m^{-3}, which are 2.3 and 3.1 times higher than those of natural nacre,[3] respectively. Other graphene-based materials just exhibit a sort of mechanical property, such as tensile strength, stiffness, and toughness. For instance, the ternary bioinspired rGO–DWNTs–PCDO nanocomposites exhibit a superior toughness of 9.2 MJ m^{-3}; however, the tensile strength is only about

 This journal is © The Royal Society of Chemistry 2016

Published on 07 October 2016. Downloaded on 06/11/2016 06:08:16.

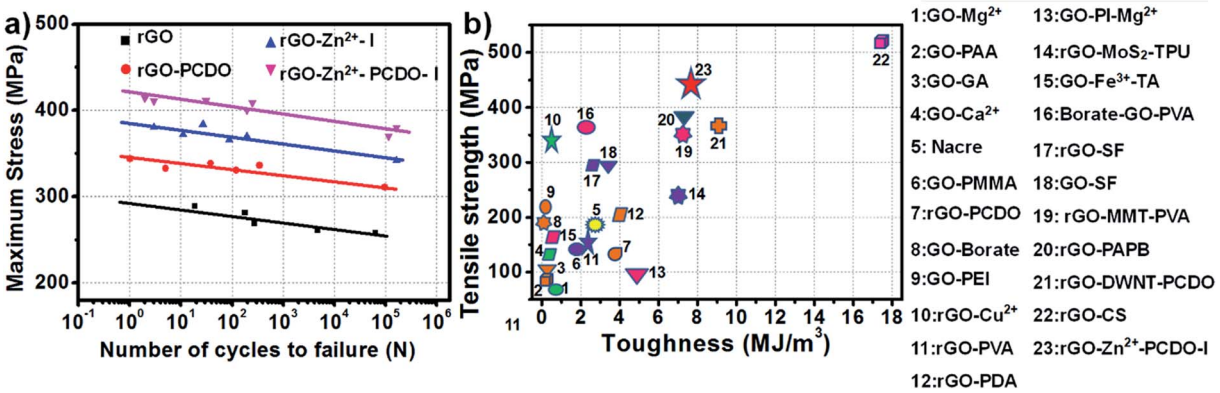

Fig. 4 (a) Tensile fatigue testing of the rGO film, rGO–PCDO, rGO–Zn^{2+}-I and rGO–Zn^{2+}–PCDO-I nanocomposites. At the same stress level, the rGO–Zn^{2+}–PCDO-I nanocomposites have longer fatigue life than other layered materials. (b) Comparison of the tensile strength and toughness of the resultant BGBNs with natural nacre[3] and other layered graphene-based materials, including ternary graphene-based nanocomposites (rGO–MoS_2–TPU,[38] rGO–DWNTs–PCDO[37] and rGO–MMT–PVA[39]), π–π conjugated interaction (rGO–PAPB),[40] hydrogen interaction (rGO–PVA,[13] GO–PMMA,[14] rGO–SF[43] and GO–SF[44]), ionic interaction (GO–Mg^{2+},[15] GO–Ca^{2+} (ref. 15) and rGO–Cu^{2+} (ref. 17)), covalent cross-linking (GO–GA,[45] GO–PEI,[46] GO–PAA,[47] GO–borate,[48] rGO–PCDO[26] and rGO–PDA[49]), and two combinations of interfacial interactions (rGO–CS,[21] GO–Fe^{3+}–TA,[42] GO–PI–Mg^{2+} (ref. 41) and borate–GO–PVA[50]).

374.1 MPa.[37] Other ternary nanocomposites, including rGO–molybdenum disulfide (MoS_2)–thermoplastic polyurethane (TPU)[38] and rGO–montmorillonite (MMT)–PVA,[39] also possess poor tensile stress or toughness, which is attributed to the relatively weak synergistic toughening effect. Another similar example is π–π conjugated interactions of rGO–poly(acrylic acid-*co*-(4-acrylamidophenyl) boronic acid) (PAPB) nanocomposites with a high toughness of 7.5 MJ m^{-3}, but the ultimate stress is about 382 MPa,[40] which is attributed to a single interfacial interaction. The ternary GO–polyimide (PI)–Mg^{2+} (ref. 41) and GO–Fe^{3+}–tannic acid (TA)[42] nanocomposites also show low mechanical properties due to only interfacial interaction of ionic bonding. Other binary nanocomposites with different interfacial interactions, such as hydrogen interactions (GO–PVA,[13] GO–PMMA,[14] rGO–silk fibroin (SF)[43] and GO–SF[44]), ionic interactions (GO–Mg^{2+},[15] GO–Ca^{2+} (ref. 15) and rGO–Cu^{2+} (ref. 17)), covalent cross-linkings (GO–glutaraldehyde (GA),[45] GO–polyetherimide (PEI),[46] GO–polyallylamine (PAA),[47] GO–borate,[48] rGO–PCDO[26] and GO–poly(dopamine) (PDA)[49]), and ternary borate–GO–PVA[50] nanocomposites, also indicate lower mechanical properties. Another noteworthy example is that the previous rGO–CS nanocomposites possess a tensile strength of 526.7 MPa and toughness of 17.7 MJ m^{-3}, respectively, higher than those of the resultant BGBNs.[21] The reason is that the rGO–CS nanocomposites possess higher crosslinking density than the rGO–Zn^{2+}–PCDO-I nanocomposites, which is attributed to more active groups of CS molecular chains than PCDO molecular chains, as well as much more CS molecule content (5.64 wt%) in rGO–CS nanocomposites than PCDO molecular chain content (2.68 wt%) in rGO–Zn^{2+}–PCDO-I nanocomposites. In brief, owing to the crack bridging of covalent cross-linking bonds and the hysteresis of Zn^{2+} ionic bonds, as well as crack deflection of rGO nanosheets, the resultant BGBNs achieve admirable mechanical properties with integration of tensile strength and toughness simultaneously. In addition, the electrical conductivity testing, as shown in Table S5,† indicates that the BGBNs have excellent electrical properties, which could enable the resultant materials to be applied in flexible electrodes of supercapacitors[51] and other intelligent devices.

Conclusion

In conclusion, inspired by the abundant interfacial interactions and hierarchical layered structure of natural nacre, we have successfully demonstrated the synergistic toughening effect from ionic and covalent cross-linking bonding for fabricating high performance bioinspired graphene-based nanocomposites (BGBNs). The resultant BGBNs show the integration of the high tensile strength and excellent toughness, exceeding natural nacre and other conventional graphene-based nanocomposites. Meanwhile, the robust BGBNs also achieve outstanding fatigue resistance performance and high electrical conductivity. These outstanding characteristics will enable these materials for many applications in fields of aerospace, flexible electrodes of supercapacitors and other intelligent devices. The study also provides an alternative strategy for the design of integrated, high-performance graphene-based nanocomposites in the future.

Methods

Materials

Crystalline graphite powder, zinc chloride solution (1 M) and 57 wt% hydroiodic acid (HI), and 10,12-pentacosadiyn-1-ol (PCDO) were purchased from Qingdao Jing Ri Lai graphite co., Ltd, Sigma-Aldrich, Tokyo Chemical Industry Co., Ltd, respectively.

Assembly of the binary GO–Zn^{2+} hybrid materials

The GO was obtained through the modified Hummers method and dispersed with deionized water, followed by stirring and ultrasonication for several minutes until the solution became

Published on 07 October 2016. Downloaded on 06/11/2016 06:08:16.

homogeneous. Then, a small quantity of diluted Zn^{2+} solution was added to the GO solution and stirred slowly and sonicated for a few more minutes. The homogenous solution was assembled into the GO–Zn^{2+} hybrid layered paper through a vacuum-assisted filtration technique.

Synthesis of rGO–Zn^{2+}–PCDO nanocomposites

First, the obtained GO–Zn^{2+} hybrid layered materials were immersed in PCDO/THF solution for two hours. Then, the GO–Zn^{2+}–PCDO nanocomposites were achieved in UV irradiation with an atmosphere of nitrogen and 365 nm wavelength. Finally, after soaking in 57 wt% HI solution for several hours, the resultant rGO–Zn^{2+}–PCDO nanocomposites were achieved by washing with water and alcohol several times and drying.

Characterization

The scanning electron microscopy (SEM) images were obtained by using a field-emission scanning electron microscope (JEOL-7500F). A Leica TCS SP5 was applied to conduct atomic force microscopy (AFM). A TG/DTA6300 was applied to perform the thermogravimetric analysis under a N_2 atmosphere and at 10 K min^{-1} heating rate. Raman spectroscopy measurements were performed with a LabRAM HR800 (Horiba Jobin Yvon) under 2.54 eV excitation energy and 488 nm wavelength. X-ray diffraction (XRD) profiles were obtained using Cu-Kα radiation ($\lambda = 1.54$ nm) with a Shimadzu LabX XRD-6000. A Shimadzu AGS-X Tester was applied to measure samples' mechanical properties in tensile mode with 1 mm min^{-1} loading rate. The samples were cut into strips with 3 mm width and 20 mm length. A source meter (Agilent E4980A) was applied to measure the electrical properties of the final artificial nacre with a two-probe approach. Tensile fatigue tests were conducted by using an Instron ElectroPuls E1000; the frequency was 1 Hz and the stress ratio (R: minimum to maximum applied stress) was 0.1 during the cyclic loading tests.

Acknowledgements

This work was supported by the Excellent Young Scientist Foundation of NSFC (51522301), the National Natural Science Foundation of China (21273017, 51103004), the Program for New Century Excellent Talents in University (NCET-12-0034), the Fok Ying-Tong Education Foundation (141045), the Open Project of Beijing National Laboratory for Molecular Sciences, the 111 Project (B14009), the Aeronautical Science Foundation of China (20145251035, 2015ZF21009), the State Key Laboratory for Modification of Chemical Fibers and Polymer Materials, Donghua University (LK1508), and the Fundamental Research Funds for the Central Universities (YWF-15-HHXY-001, and YWF-16-BJ-J-09).

References

1 F. Barthelat and R. Rabiei, *J. Mech. Phys. Solids*, 2011, **59**, 829–840.
2 S. Keten, Z. Xu, B. Ihle and M. J. Buehler, *Nat. Mater.*, 2010, **9**, 359–367.
3 M. A. Meyers, J. McKittrick and P.-Y. Chen, *Science*, 2013, **339**, 773–779.
4 F. Barthelat, Z. Yin and M. J. Buehler, *Nat. Rev. Mater.*, 2016, **1**, 16007.
5 A. Khayer Dastjerdi, R. Rabiei and F. Barthelat, *J. Mech. Behav. Biomed. Mater.*, 2013, **19**, 50–60.
6 H. B. Yao, H. Y. Fang, X. H. Wang and S. H. Yu, *Chem. Soc. Rev.*, 2011, **40**, 3764–3785.
7 X. Huang, Z. Yin, S. Wu, X. Qi, Q. He, Q. Zhang, Q. Yan, F. Boey and H. Zhang, *Small*, 2011, **7**, 1876–1902.
8 J. Wang, Q. Cheng and Z. Tang, *Chem. Soc. Rev.*, 2012, **41**, 1111–1129.
9 D. Li and R. B. Kaner, *Science*, 2008, **320**, 1170–1171.
10 D. A. Dikin, S. Stankovich, E. J. Zimney, R. D. Piner, G. H. B. Dommett, G. Evmenenko, S. T. Nguyen and R. S. Ruoff, *Nature*, 2007, **448**, 457–460.
11 Y. Zhang, S. Gong, Q. Zhang, P. Ming, S. Wan, J. Peng, L. Jiang and Q. Cheng, *Chem. Soc. Rev.*, 2016, **45**, 2378–2395.
12 S. Wan, J. Peng, L. Jiang and Q. Cheng, *Adv. Mater.*, 2016, **28**, 7862–7898.
13 Y. Q. Li, T. Yu, T. Y. Yang, L. X. Zheng and K. Liao, *Adv. Mater.*, 2012, **24**, 3426–3431.
14 K. W. Putz, O. C. Compton, M. J. Palmeri, S. T. Nguyen and L. C. Brinson, *Adv. Funct. Mater.*, 2010, **20**, 3322–3329.
15 S. Park, K.-S. Lee, G. Bozoklu, W. Cai, S. T. Nguyen and R. S. Ruoff, *ACS Nano*, 2008, **2**, 572–578.
16 C. N. Yeh, K. Raidongia, J. Shao, Q. H. Yang and J. Huang, *Nat. Chem.*, 2015, **7**, 166–170.
17 J. Hwang, T. Yoon, S. H. Jin, J. Lee, T. S. Kim, S. H. Hong and S. Jeon, *Adv. Mater.*, 2013, **25**, 6724–6729.
18 V. Georgakilas, J. N. Tiwari, K. C. Kemp, J. A. Perman, A. B. Bourlinos, K. S. Kim and R. Zboril, *Chem. Rev.*, 2016, **116**, 5464–5519.
19 Q. Cheng, L. Jiang and Z. Tang, *Acc. Chem. Res.*, 2014, **47**, 1256–1266.
20 K. E. Prasad, B. Das, U. Maitra, U. Ramamurty and C. N. R. Rao, *Proc. Natl. Acad. Sci. U. S. A.*, 2009, **106**, 13186–13189.
21 S. Wan, J. Peng, Y. Li, H. Hu, L. Jiang and Q. Cheng, *ACS Nano*, 2015, **9**, 9830–9836.
22 S.-M. Lee, E. Pippel, U. Gösele, C. Dresbach, Y. Qin, C. V. Chandran, T. Bräuniger, G. Hause and M. Knez, *Science*, 2009, **324**, 488–492.
23 G. W. Bryan and P. E. Gibbs, *J. Mar. Biol. Assoc. U. K.*, 1979, **59**, 969–973.
24 P. E. Gibbs and G. W. Bryan, *J. Mar. Biol. Assoc. U. K.*, 1980, **60**, 205–214.
25 W. Zheng, R. Tan, L. Zhao, Y. Chen, C. Xiong and D. Yin, *RSC Adv.*, 2014, **4**, 11732–11739.
26 Q. Cheng, M. Wu, M. Li, L. Jiang and Z. Tang, *Angew. Chem., Int. Ed.*, 2013, **52**, 3750–3755.
27 I. W. P. Chen, R. Liang, H. Zhao, B. Wang and C. Zhang, *Nanotechnology*, 2011, **22**, 485708.
28 M.-M. Qin, W. Ji, Y.-Y. Feng and W. Feng, *Chin. Phys. B*, 2014, **23**, 028103.

 This journal is © The Royal Society of Chemistry 2016

Published on 07 October 2016. Downloaded on 06/11/2016 06:08:16.

29 Y.-T. Liu, M. Dang, X.-M. Xie, Z.-F. Wang and X.-Y. Ye, *J. Mater. Chem.*, 2011, **21**, 18723–18729.
30 Y.-T. Liu, Q.-P. Feng, X.-M. Xie and X.-Y. Ye, *Carbon*, 2011, **49**, 3371–3375.
31 Y. T. Liu, X. D. Zhu, Z. Q. Duan and X. M. Xie, *Chem. Commun.*, 2013, **49**, 10305–10307.
32 J. P. Gong, Y. Katsuyama, T. Kurokawa and Y. Osada, *Adv. Mater.*, 2003, **15**, 1155–1158.
33 Y. Liu, B. Xie and Z. Xu, *J. Mater. Chem.*, 2011, **21**, 6707–6712.
34 T. L. Sun, T. Kurokawa, S. Kuroda, A. B. Ihsan, T. Akasaki, K. Sato, M. A. Haque, T. Nakajima and J. P. Gong, *Nat. Mater.*, 2013, **12**, 932–937.
35 J. Y. Sun, X. Zhao, W. R. K. Illeperuma, O. Chaudhuri, K. H. Oh, D. J. Mooney, J. J. Vlassak and Z. Suo, *Nature*, 2012, **489**, 133–136.
36 K. J. Henderson, T. C. Zhou, K. J. Otim and K. R. Shull, *Macromolecules*, 2010, **43**, 6193–6201.
37 S. Gong, W. Cui, Q. Zhang, A. Cao, L. Jiang and Q. Cheng, *ACS Nano*, 2015, **9**, 11568–11573.
38 S. Wan, Y. Li, J. Peng, H. Hu, Q. Cheng and L. Jiang, *ACS Nano*, 2015, **9**, 708–714.
39 P. Ming, Z. Song, S. Gong, Y. Zhang, J. Duan, Q. Zhang, L. Jiang and Q. Cheng, *J. Mater. Chem. A*, 2015, **3**, 21194–21200.
40 M. Zhang, L. Huang, J. Chen, C. Li and G. Shi, *Adv. Mater.*, 2014, **26**, 7588–7592.
41 J.-Y. Kong, M.-C. Choi, G. Y. Kim, J. J. Park, M. Selvaraj, M. Han and C.-S. Ha, *Eur. Polym. J.*, 2012, **48**, 1394–1405.
42 R.-Y. Liu and A.-W. Xu, *RSC Adv.*, 2014, **4**, 40390–40395.
43 K. Hu, L. S. Tolentino, D. D. Kulkarni, C. Ye, S. Kumar and V. V. Tsukruk, *Angew. Chem., Int. Ed.*, 2013, **52**, 13784–13788.
44 Y. Yin, K. Hu, A. M. Grant, Y. Zhang and V. V. Tsukruk, *Langmuir*, 2015, **31**, 10859–10870.
45 Y. Gao, L.-Q. Liu, S.-Z. Zu, K. Peng, D. Zhou, B.-H. Han and Z. Zhang, *ACS Nano*, 2011, **5**, 2134–2141.
46 Y. Tian, Y. Cao, Y. Wang, W. Yang and J. Feng, *Adv. Mater.*, 2013, **25**, 2980–2983.
47 S. Park, D. A. Dikin, S. T. Nguyen and R. S. Ruoff, *J. Phys. Chem. C*, 2009, **113**, 15801–15804.
48 Z. An, O. C. Compton, K. W. Putz, L. C. Brinson and S. T. Nguyen, *Adv. Mater.*, 2011, **23**, 3842–3846.
49 W. Cui, M. Li, J. Liu, B. Wang, C. Zhang, L. Jiang and Q. Cheng, *ACS Nano*, 2014, **8**, 9511–9517.
50 L. Liu, Y. Gao, Q. Liu, J. Kuang, D. Zhou, S. Ju, B. Han and Z. Zhang, *Small*, 2013, **9**, 2466–2472.
51 X. Huang, Z. Zeng, Z. Fan, J. Liu and H. Zhang, *Adv. Mater.*, 2012, **24**, 5979–6004.